Editors' Suggestion

Magnetic-field-induced topological phase transition in Fe-doped $(Bi,Sb)_2Se_3$ heterostructures

Y. Satake,[1,2] J. Shiogai,[1,*] G. P. Mazur,[2] S. Kimura,[1] S. Awaji,[1] K. Fujiwara,[1] T. Nojima,[1] K. Nomura,[1,3] S. Souma,[3,4] T. Sato,[3,4,5] T. Dietl,[2,4] and A. Tsukazaki[1,3]

[1]*Institute for Materials Research, Tohoku University, Sendai 980-8577, Japan*

[2]*International Research Centre MagTop, Institute of Physics, Polish Academy of Sciences, Aleja Lotnikow 32/46, PL-02668 Warsaw, Poland*

[3]*Center for Spintronics Research Network (CSRN), Tohoku University, Sendai 980-8577, Japan*

[4]*WPI-Advanced Institute for Materials Research, Tohoku University, Sendai 980-8577, Japan*

[5]*Department of Physics, Tohoku University, Sendai 980-8578, Japan*

(Received 2 October 2019; revised manuscript received 2 February 2020; accepted 6 March 2020; published 21 April 2020)

Three-dimensional topological insulators (3D TIs) possess a specific topological order of electronic bands, resulting in gapless surface states via bulk-edge correspondence. Exotic phenomena have been realized in ferromagnetic TIs, such as the quantum anomalous Hall (QAH) effect with a chiral-edge conduction and a quantized value of the Hall resistance R_{yx}. Here, we report on the emergence of distinct topological phases in paramagnetic Fe-doped $(Bi,Sb)_2Se_3$ heterostructures with varying structure architecture, doping, and magnetic and electric fields. Starting from a 3D TI, a two-dimensional insulator appears at layer thicknesses below a critical value, which turns into an Anderson insulator for Fe concentrations sufficiently large to produce localization by magnetic disorder. With applying a magnetic field, a topological transition from the Anderson insulator to the QAH state occurs, which is driven by the formation of an exchange gap owing to a giant Zeeman splitting and reduced magnetic disorder. A topological phase diagram of $(Bi,Sb)_2Se_3$ allows exploration of intricate interplay of topological protection, magnetic disorder, and exchange splitting.

DOI: 10.1103/PhysRevMaterials.4.044202

I. INTRODUCTION

Three-dimensional topological insulators (3D TIs) are a class of matter that is composed of gapless surface states and insulating bulk [1–3]. In such material systems, various types of topological phase transitions (TPTs) are expected to appear as a result of structural modifications and application of external fields [4–13]. For instance, an exchange gap formation in the surface states engenders a TPT, which leads to the quantum anomalous Hall (QAH) phase, i.e., to the Chern insulator. In this phase, similarly to the conventional quantum Hall effect (QHE), charge transport proceeds via a dissipationless chiral-edge channel while the origin is completely different [14–16]; the QAH effect is driven by the formation of an exchange gap and the QHE by Landau level splitting. To materialize the QAH phase in TIs, the surface electronic states should be modified by the exchange gap owing to some mechanisms as follows: (1) coupling between surface state and ferromagnetically aligned spins of transition metal impurities [15–17] or aligned spins by external magnetic field in the antiferromagnetic topological insulator [18,19], (2) proximity coupling effect with adjacent magnetic moment [20–22], or (3) band crossing driven by a Zeeman splitting [17,23]. To date, experimental observations of the QAH effect have been accomplished for Cr-doped or V-doped $(Bi,Sb)_2Te_3$ (BST) 3D TI films, where a perpendicular spontaneous magnetization develops below the Curie temperature [type (1)] [15,16,24–28], and for a proximitized $(Bi,Sb)_2Te_3$/ferromagnetic insulator heterostructure [type (2)] [29]. In contrast, the QAH type (3) has not been observed in paramagnetic $(Bi,Sb)_2Se_3$-based TIs, whereas the quantization of the Hall resistance is accomplished by the application of a magnetic field to a four-quintuple layer of Cr-doped $(Bi,Sb)_2Te_3$ [30], Ti-doped $(Bi, In)_3Te_2$ [31], and $MnBi_2Te_4$ [18,19].

As another TPT, the surface state can be gapped when the 3D-TI film is sufficiently thin to activate hybridization of states from the opposite surfaces [1,2]. Thin films of Bi_2Se_3-type 3D TIs are known to be two-dimensional (2D) trivial insulators [4,32–34] when the hybridization is sufficiently strong, as presented in Fig. 1(a). Considering this trivial electronic band as an initial state, the giant Zeeman splitting generated by an external magnetic field produces a specific band crossing [Fig. 1(b)] with formation of an exchange gap [Fig. 1(c)] [17,23] at this crossing point, equivalent to that driven by types (1) and (2) in coupling with ferromagnetic systems, inducing a conceptually different type (3) of QAH. To illustrate the topological phase transition from the hybridized insulator to the QAH phase driven by the Zeeman splitting, we have calculated the band structure using a 3D-TI slab geometry. Figures 1(d)–1(f) demonstrate the band modification of 3D TI by the intersurface hybridization and the Zeeman effect. When Δ_{hy} is larger than Δ_{Zeeman}, the hybridized insulator is stabilized without surface gapless states [Fig. 1(d)]. The Δ_{Zeeman} exceeding Δ_{hy} forms a nontrivial exchange gap with a one-dimensional chiral-edge channel as shown in Figs. 1(e) and 1(f), with gap size proportional to the magnetic field. In

*Corresponding author: junichi.shiogai@imr.tohoku.ac.jp

 ©2020 American Physical Society

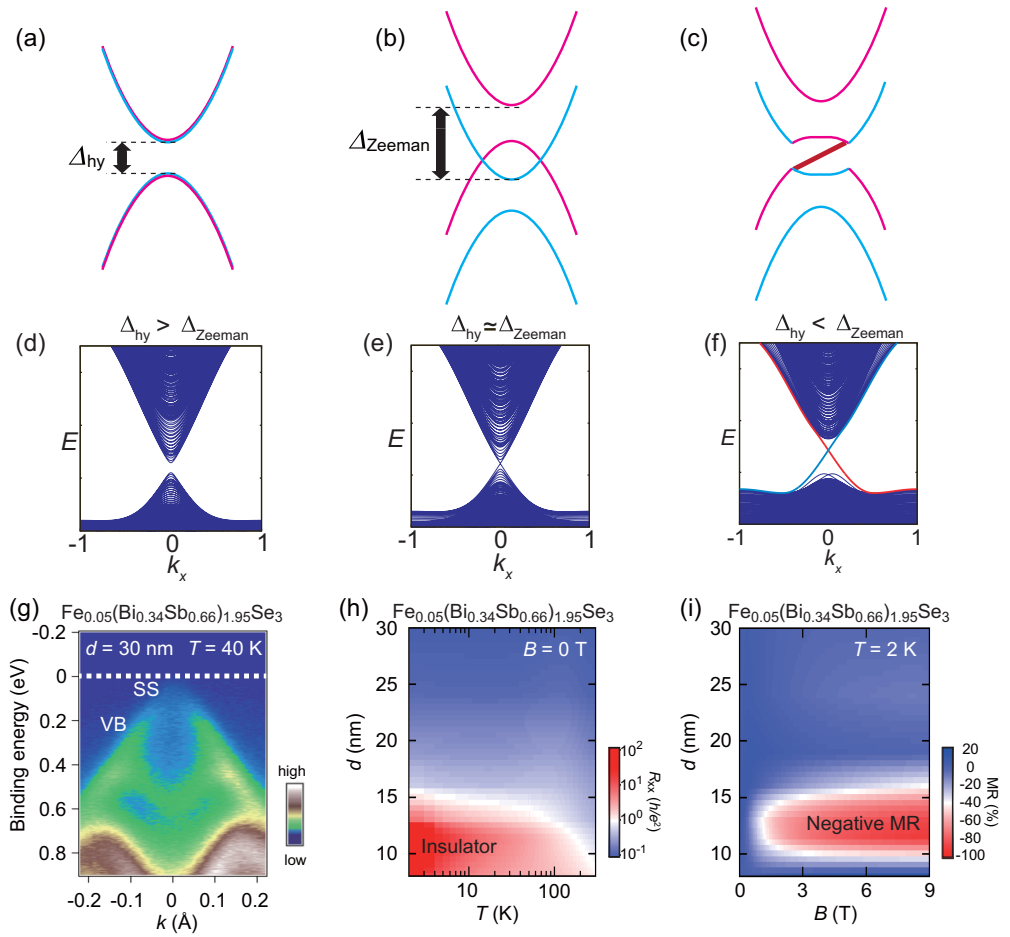

FIG. 1. (a)–(c) Evolution of surface spin subband structure in paramagnetic Fe-doped $(Bi,Sb)_2Se_3$ thin films upon thickness reduction and external magnetic field application. (a) Surface states of spin-up (magenta) and spin-down (cyan) subbands with gap Δ_{hy} driven by intersurface hybridization, leading to 2D insulator phase. (b) Under an external perpendicular magnetic field, the spin subband degeneracy is lifted by the Zeeman effect, producing band crossing when the Zeeman energy Δ_{Zeeman} exceeds Δ_{hy}. (c) At crossings of spin-up (magenta) and spin-down (cyan) bands, a gap is generated by the spin-orbit interaction, leaving a one-dimensional chiral-edge channel in the bulk band gap (red solid line). (d)–(f) Calculated electronic band structure of three-dimensional topological insulator thin films. The band structure is calculated using the 3D-TI slab for cases in which (d) Δ_{hy} is larger than Δ_{Zeeman}, (e) Δ_{hy} is comparable to Δ_{Zeeman}, and (f) Δ_{Zeeman} is larger than Δ_{hy}. (g) ARPES intensity of the 30-nm-thick $Fe_{0.05}(Bi_{0.34}Sb_{0.66})_{1.95}Se_3$/3-nm-thick Bi_2Se_3 film around the $\bar{\Gamma}$ point measured at $T = 40$ K. SS and VB, respectively, represent surface state and bulk valence band. E_F is indicated by a white dashed line. (h) Longitudinal resistance R_{xx} of $Fe_{0.05}(Bi_{0.34}Sb_{0.66})_{1.95}Se_3/Bi_2Se_3$ at $B = 0$ as a function of the magnetic layer thickness d and temperature T. Color bar scale is in units of h/e^2. (i) Magnetoresistance of $Fe_{0.05}(Bi_{0.34}Sb_{0.66})_{1.95}Se_3/Bi_2Se_3$ at 2 K as a function of d and B. Color scale bar corresponds to +20% (blue) to −100% (red).

Fig. 1(f), the red (blue) thick curve shows the chiral-edge mode at one (the other) edge.

With a minor contribution of the ordinary Hall effect under magnetic field owing to Fermi energy (E_F) locating in the gap, the magnetic-field-induced anomalous Hall effect plays a critical role for the quantization of the Hall conductivity. This study demonstrates the presence of TPTs between 3D TI, a two-dimensional (2D) insulator, and QAH phases in paramagnetic Fe-doped Bi_2Se_3-based heterostructures by controlling Fe doping and layer thickness and by application of external magnetic and electric fields.

The tetradymite compound Bi_2Se_3 is a representative 3D TI, in which a large bulk band gap (approximately 300 meV) hosts gapless surface states [35]. Using angle-resolved photoemission spectroscopy (ARPES) of surface states, 50-meV gap formation was detected in paramagnetic Fe-doped bulk Bi_2Se_3; it was assigned to breakage of the time-reversal symmetry by exchange interactions [36]. Effects of magnetic impurities upon topological surface states were also studied by *in situ* deposition of Fe atoms [37–39]. It was found that Fe acts as a donor [37,38] if deposited at room temperature but as an acceptor if deposited at 8 K [38]. A question on whether the presence of a Fe surface layer opens a gap or not in the topological states was also examined experimentally and theoretically [37–39].

According to one theoretical proposal, Fe-doped Bi_2Se_3-based heterostructures are a preferred platform for observing the emergence of the QAH phase [17]. Nevertheless, no QAH effect has yet been observed in magnetically doped Bi_2Se_3-based films, probably because of the absence or weakness

of the ferromagnetic ordering, and associated difficulties in tuning of the E_F into a correspondingly small exchange gap [40]. In contrast, a TPT from the TI to the 2D insulator by film thickness reduction was demonstrated for Bi_2Se_3 films using ARPES and electrical measurements [4,31–33]. Depending on the experimental method used, the critical thickness for the transition has been reported as 5 [4] or 10 nm [41] in Bi_2Se_3. For other 3D TIs such as Bi_2Te_3, $(Bi,Sb)_2Te_3$ (BST) and magnetically doped BST films, variations in the strength of the spin-orbit interaction are thought to account for critical thickness changes from 1 to 13 nm [12,42].

II. EXPERIMENTAL DETAILS

Employing molecular-beam epitaxy (MBE) and a 3-nm-thick *n*-type Bi_2Se_3 buffer layer on a semi-insulating Fe-doped InP (111) substrate, we have grown $Fe_x(Bi_{1-y}Sb_y)_{2-x}Se_3$ films of thickness d ranging from 8 to 30 nm (see Supplemental Material, Sec. 1 [43]). The control parameters are the Sb composition and the gate bias voltage for changing the E_F position [44,45], whereas the Fe concentration and the external magnetic field serve for tuning magnetic disorder and the band splitting state. Because Fe doping up to at least $x = 0.1$ (nominal composition controlled by the beam flux ratio) produces rather minor changes in R_{xx} and $|R_{yx}|$ magnitudes (see Supplemental Material, Sec. 2 [43]), we infer that Fe ions are isoelectronic impurities occupying Bi or Sb sites, and assume the same Fe^{3+} charge configuration with bulk Fe-doped Bi_2Se_3 [36] that typically corresponds to the high spin $S = 5/2$. However, Fe acts not only as a magnetic impurity, but also as an isoelectronic dopant, in a manner similar to Sb, which affects the carrier concentration owing to band shifts with respect to defect formation levels. Moreover, thickness d plays a crucially important role in the control of both (i) hybridization between surface and interfacial topological states and (ii) the width of the depletion layer in the *p-n* junction that forms at the interface of the *n*-type Bi_2Se_3 buffer layer.

III. RESULTS AND DISCUSSION

A. Angle-resolved photoemission spectroscopy (ARPES) and magnetic properties

We have characterized the electronic structure of a 30-nm-thick $Fe_{0.05}(Bi_{0.34}Sb_{0.66})_{1.95}Se_3/Bi_2Se_3$ heterostructure at 40 K using ARPES. As presented in Fig. 1(g), the topological surface states and the bulk valence band are resolved clearly at the Γ point, indicating that this thick Fe-doped $(Bi,Sb)_2Se_3$ layer preserves key features of 3D TIs and does not engender a substantial Fermi level shift. Linear dispersion of the surface band is more readily apparent when moving the Fermi level up in energy by an aging process that increases the surface electron concentration (see Fig. S3 in the Supplemental Material [43]). Contrary to an earlier report on ARPES at 10 K of bulk Fe-doped Bi_2Se_3 samples with Fe concentration $x = 0.12$ and 0.16, which was considered as a consequence of ferromagnetic ordering [36], no sizable gap in the surface states is resolved in the case of our MBE-grown layer with $x = 0.05$; this indicates the absence of a long range magnetic order at the Fe concentration of interest here.

The ARPES data are consistent with the magnetotransport studies: neither hysteretic nor saturation behavior has been observed in our Hall effect measurements, indicating that Fe ions remain in a paramagnetic phase down to 2 K for $x = 0.05$. This is in agreement with previous direct measurements of magnetization $M(T,H)$ down to 2 K and up to $\mu_0 H = 5\,T$ on bulk samples that showed paramagnetic behavior below $x = 0.16$ [36]. Some hysteresis superimposed on the paramagnetic signal $M(H)$ was detected for $x \geqslant 0.16$ at 2 K [36]. The absence of ferromagnetism at low Fe concentrations is consistent with our direct magnetization measurements employing a superconducting quantum interference device (SQUID), which does not show any hysteresis. However, a quantitative evaluation of the epilayer paramagnetic signal from our SQUID and electron paramagnetic resonance studies has been hampered by a small thickness of the epilayers and a large magnetic contribution of the Fe-doped InP substrate. The absence of ferromagnetism in the Fe-doped Bi_2Se_3 is also consistent with *ab initio* studies [46,47].

B. Magnetotransport properties

The values of the 2D resistivity tensor components, i.e., the sheet resistance R_{xx} and the Hall resistance R_{yx}, have been measured in the Hall-bar geometry and using a standard lock-in technique [43]. Figure 1(h) presents a contour plot of R_{xx} values for $Fe_{0.05}(Bi_{0.34}Sb_{0.66})_{1.95}Se_3/Bi_2Se_3$ films in $B = 0$ as a function of layer thickness d and temperature T (see Supplemental Material, Fig. S4(a), for a detailed data set [43]). One phenomenological criterion describing the critical point of the localization transition in the 2D case is the sheet resistance value of $h/e^2 \cong 25.8\,k\Omega$ [48,49]. The boundary is indicated as the white region in Fig. 1(h). As shown there, $R_{xx}(T)$ determined for the 30-nm-thick film shows lower values than those of h/e^2, in addition to weak temperature dependence, implying that this sample is the 3D-TI phase [Fig. 1(g)]. With decreasing d at fixed Fe and Sb concentrations ($x = 0.05$ and $y = 0.66$), $R_{xx}(T)$ reaches the critical value of h/e^2 at a thickness of $d = 14\,nm$, below which dependence $R_{xx}(T)$ exhibits insulating behavior and R_{xx} magnitudes exceed 1 MΩ at the lowest temperature of 2 K [deep-red region in Fig. 1(h)]. Such highly insulating features at $d < 14$ nm can be ascribed either to the trivial Anderson insulator [50,51] or to the quantum spin Hall insulator [51,52], if the formation of edge states would accompany hybridization of surface states. However, edge conductance would hardly dominate the charge transport in the present Hall-bar geometry with the channels longer than the expected protection length of helical topological channels. The phase coherence length estimated by weak antilocalization analysis of the Bi_2Se_3 thin films is about 200 nm [45], which is well below the channel length. In principle, ARPES is an effective way to tell the topological phase. However, the high resistance and the corresponding charging effect made it difficult to assess the electronic structure of our thinnest samples. Nevertheless, the critical thickness we found for this 2D insulator is rather thick compared to the values (5–10 nm) reported for nonmagnetic Bi_2Se_3 films [4,41]. This point can be explained by the empirical fact (see Supplemental Material, Sec. 5 [43]) that the substitution of heavier Bi or Sb by lighter Fe reduces the spin-orbit

interaction strength, which might increase the critical thickness. Furthermore, the presence of the n-type Bi_2Se_3 buffer layer depletes the p-type $Fe_{0.05}(Bi_{0.34}Sb_{0.66})_{1.95}Se_3$ layer [45], making the effective thickness less than the nominal value.

More importantly, in our paramagnetic samples, spin disorder scattering by Fe impurities can be effective for expanding the Anderson insulator range with regard to the thickness and temperature of $Fe_x(Bi_{1-y}Sb_y)_{2-x}Se_3$ films [Fig. 1(h)], making it wider compared to Bi_2Se_3. Temperature dependence of resistivity for samples with $d = 14$ nm and various x are presented in Fig. S2 in the Supplemental Material [43]. The data clearly show a transition from the weakly localized regime to the strongly localized regime, characterized by a sharp increase of resistivity on lowering temperature, which appears at $x > 0.04$. As expected in the absence of Landau quantization and in the 2D case [53], this transition has a crossover character, so that it does not obey scaling equations. As presented in Fig. 1(i), the magnitude of magnetoresistance defined as $\mathrm{MR} = [R_{xx}(B) - R_{xx}(0)]/R_{xx}(0)$ exceeds -80% in 9 T and at 2 K in the vicinity of the localization transition. The ordering of Fe spins in the magnetic field reduces magnetic disorder and enhances the spin splitting of electronic states. Consequently, a QAH phase would appear in the thickness region toward type (3) by the application of the magnetic field as schematically shown in Figs. 1(c) and 1(f). In accordance with the expectation that reduction of magnetic disorder occurs for any field direction, we find negative MR to be also present for the in-plane magnetic field (Supplemental Material, Fig. S6 [43]).

Figure 2 presents a dependence of Hall resistance R_{yx} on the Sb concentration y at $T = 2$ K and $B = 9$ T for $Fe_{0.05}(Bi_{1-y}Sb_y)_{1.95}Se_3/Bi_2Se_3$ with $d \cong 14$ nm (red circles). This dependence is strikingly different compared to the case of nonmagnetic $(Bi_{1-y}Sb_y)_2Se_3/Bi_2Se_3$ films with $d = 14-20$ nm (black squares) [44]. The representative raw data of $R_{yx}(B)$ for Fe-doped samples are shown in the inset. For nonmagnetic $(Bi_{1-y}Sb_y)_2Se_3/Bi_2Se_3$, the sign reversal of R_{yx} reflects the conversion of the carrier type and therefore the tuning of E_F across the charge neutrality point (CNP), which appears at $y \cong 0.7$. In contrast for the Fe-doped films, the positive value of R_{yx} persists in $y > 0.5$, indicating that the positive contribution of magnetic-field-induced anomalous Hall resistance is much larger than the negative contribution of the ordinary Hall component; empirically $R_{yx} = R_0B + R_AM_z$ where R_0 is the ordinary Hall coefficient, B magnetic field, R_A the anomalous Hall coefficient, and M_z the out-of-plane component of magnetization. By application of a perpendicular B, B-induced M_z dominantly contributes to the R_{yx} with a negligibly small ordinary component. Moreover, R_{yx} is enhanced greatly with a peak at $y \cong 0.67$, close to the CNP in nonmagnetic films. The behavior of R_{yx} as a function of y, together with a large magnitude of R_{yx} at the CNP, demonstrates that R_{yx} is dominated by the intrinsic anomalous Hall effect, as its amplitude is expected to be dependent on the E_F position while its sign is determined by magnetization direction and exchange coupling [17,19,54]. In fact, the tangent of the Hall angle R_{yx}/R_{xx} approaches unity at values greater than $d = 14$ nm (see Supplemental Material, Fig. S4(f) [43]) indicating that the condition for the Landau quantization of the density of states, $R_0B/R_{xx} > 1$, is not met. It should be noted that such a large R_{yx} at $d = 14$ nm is observed also in the insulator region [Fig. 1(h)], where negative MR exists [Fig. 1(i)].

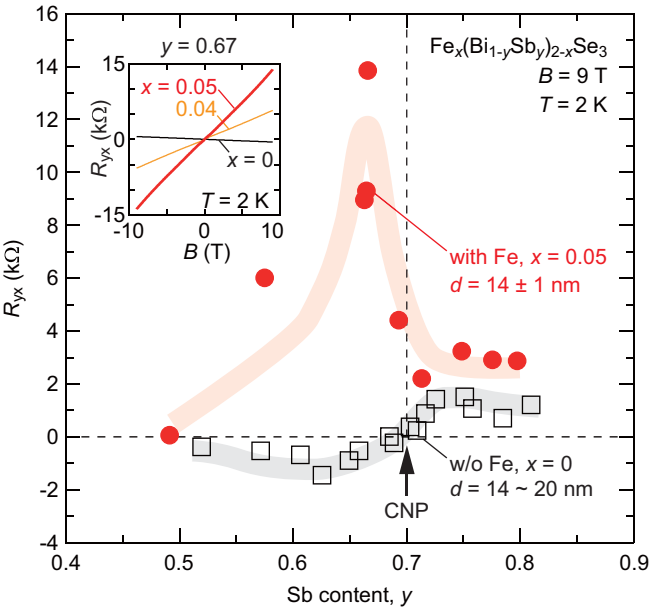

FIG. 2. Hall resistance of Fe-doped and nonmagnetic heterostructures against Sb composition y at 9 T and 2 K. Hall resistances R_{yx} of 14-nm-thick $Fe_x(Bi_{1-y}Sb_y)_{2-x}Se_3$/3-nm-thick Bi_2Se_3 (red circles) dominated by the anomalous component and those of 14–20-nm-thick nonmagnetic $(Bi_{1-y}Sb_y)_2Se_3$/3-nm-thick Bi_2Se_3 films (black squares) are shown against Sb content y. CNP denotes the charge neutral point of nonmagnetic samples. The inset shows the Hall effect measurement for $Fe_x(Bi_{0.33}Sb_{0.67})_{2-x}Se_3$/3-nm-thick Bi_2Se_3 films for Fe content $x = 0$ (solid black line), 0.04 (orange), and 0.05 (red).

Together with revealing enhanced values of $R_{yx}(B)$, transition behavior is found in $R_{xx}(T)$ in elevated fields up to 24 T, as depicted in Fig. 3(a). The field-induced insulator-metal transition becomes apparent below 50 K. For $B > 12$ T, the metallicity increases concomitantly with increasing B down to temperatures as low as 1.6 K. The criterion in $B = 9$ T for the sign change of dR_{xx}/dT being close to 0.5 h/e^2. This value for the metal-insulator transition (MIT), compared to 1 h/e^2 for MIT driven by structural modifications [cf. Fig. 1(h)], indicates one other type of the TPT. We attributed this field-induced metallization to a TPT from the 2D insulator to a QAH phase. The insulator at $B = 0$ with hybridization gap Δ_{hy} [Figs. 1(a) and 1(d)] changes to be a state with inverted bands by Zeeman splitting Δ_{Zeeman} when $\Delta_{Zeeman} > \Delta_{hy}$. With the assistance of spin-orbit coupling, a gap is formed at the crossings of surface bands hosting carriers with opposite spin orientations [17,30], as depicted in Figs. 1(c) and 1(f). Furthermore, at $\Delta_{Zeeman} > \Delta_{hy}$, gapless disorder-protected chiral channels are formed, in full analogy to the theoretical proposal for the QAH effect [17].

Having observed the signature of this TPT, we study $R_{xx}(B)$ and $R_{yx}(B)$ at $T = 1.6$ K employing a field-effect transistor (FET) device for precise tuning of E_F. The FET layout is depicted in the inset shown with Fig. 3(b) (see also Supplemental

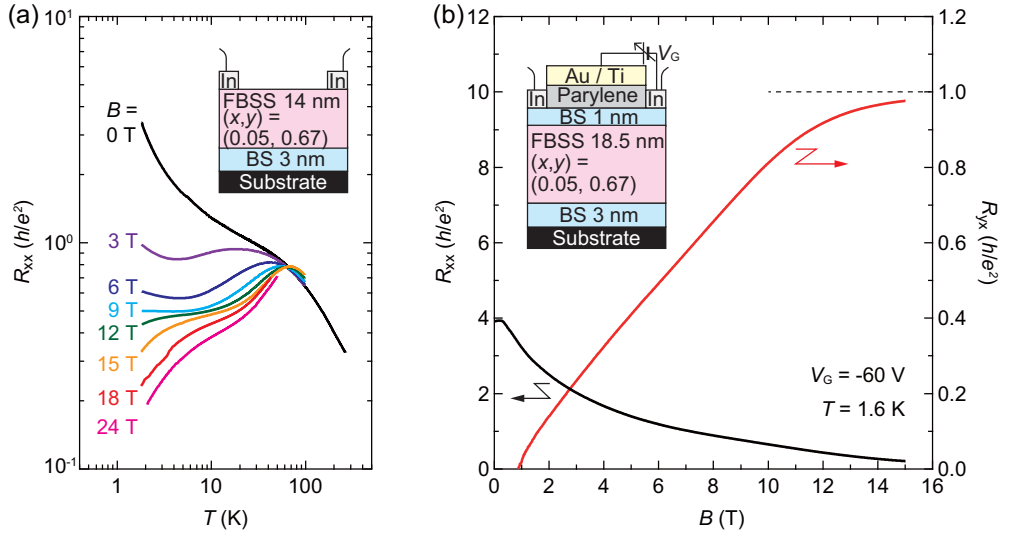

FIG. 3. Magnetic-field-induced insulator-metal transition and quantum anomalous Hall effect. (a) Longitudinal sheet resistance $R_{xx}(T)$ of 14-nm-thick $Fe_{0.05}(Bi_{0.33}Sb_{0.67})_{1.95}Se_3/Bi_2Se_3$ heterostructure (inset) in various magnetic fields B. (b) Hall and sheet resistances, $R_{yx}(B)$ (solid red line) and $R_{xx}(B)$ (solid black line), measured for a FET device (shown in the inset) at $V_G = -60$ V and $T = 1.6$ K. The R_{yx} data below 1 T were not obtained owing to the large value of R_{xx}.

Material [43]); it consists of a 1-nm-thick Bi_2Se_3/18.5-nm-thick $Fe_{0.05}(Bi_{0.33}Sb_{0.67})_{1.95}Se_3$/3-nm-thick Bi_2Se_3 trilayer structure. As depicted in Fig. 3(b), by sweeping magnetic field up to 15 T under $V_G = -60$ V, the large R_{xx} value of 3.92 h/e^2 in $B = 0$ (black line) decreases monotonically to 0.2 h/e^2 whereas R_{yx} (red line) increases, reaching 0.975 h/e^2, i.e., almost the value expected for the ideal QAH phase, h/e^2. Consequently, the magnetic-field-induced transition from the 2D insulator to the QAH phase can be observed clearly at the high temperature of $T = 1.6$ K, at which the quantization accuracy of the R_{yx} value is comparable to that reported for Cr modulation-doped $(Bi,Sb)_2Te_3$ heterostructures [15,55] and higher than that for Cr-doped or V-doped $(Bi,Sb)_2Te_3$ thin films [8,24–28]. Note that this quantization is hardly considered to be QHE due to the insulating initial state at $B = 0$ with a negligible ordinary Hall effect. The electrostatic tuning of the E_F position with respect to the gap around the CNP promotes other TPTs as presented in the conductivity tensor in the Supplemental Material, Fig. S10 [43].

The nature of relevant phases is assessed by examining the renormalization group flow of the conductivity tensor components $[\sigma_{xx} = R_{xx}/(R_{xx}^2 + R_{yx}^2),\ \sigma_{xy} = R_{yx}/(R_{xx}^2 + R_{yx}^2)]$ as a function of temperature [8,25,56]. Figures 4(a) and 4(b) show $\sigma_{xx}(T)$ and $\sigma_{xy}(T)$ for various B at $V_G = -60$ V. As T decreases, all $\sigma_{xx}(T)$ values decrease, irrespective of B. However, $\sigma_{xy}(T)$ goes to e^2/h and to zero, respectively, in high and low fields, with a crossover point of about $0.5\,e^2/h$. These data are shown in the $[\sigma_{xy}(B), \sigma_{xx}(B)]$ plane in Fig. 4(c). By lowering T from 15 K (open symbols) to 1.6 K (filled symbols) under various magnetic fields, the data converge to either $(\sigma_{xx}, \sigma_{xy}) = (0, 0)$ for the insulator or $(0, e^2/h)$ for QAH phase. The finding of a converging point in our Fe-doped $(Bi,Sb)_2Se_3$ samples clearly evidences the presence of a phase transition driven by the magnetic field, with the critical field of 7–8 T corresponding to the point at which Δ_{Zeeman} becomes comparable to Δ_{hy}. Moreover, as shown in the Supplemental Material, Fig. S10 [43], the transition driven by an electric field in fixed magnetic fields of 9 and 12 T is visible. Given the experimental observation of the TPT in the accessible magnetic field, the large g factor of the surface state should be taken into consideration to estimate Δ_{Zeeman}, as discussed in the Supplemental Material, Sec. 9 [43]. The Zeeman splitting (g factor of $Bi_2Se_3 \sim 18 - 50$ [57,58]) can

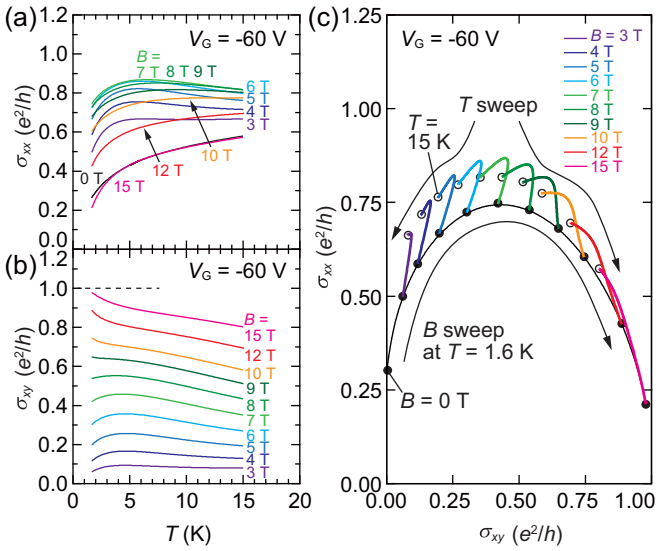

FIG. 4. Magnetic-field-induced insulator-QAH phase transition. (a),(b) Temperature dependences of the longitudinal and Hall conductivities (σ_{xx} and σ_{xy}) at $V_G = -60$ V for various magnetic fields B. (c) Renormalization group flow in the $[\sigma_{xx}(T), \sigma_{xy}(T)]$ plane in various B from 3 to 15 T. Each curve is extracted from data in (a),(b) employing the same color code. Empty and filled circles, respectively, present data obtained at $T = 15$ and 1.6 K. The $[\sigma_{xx}, \sigma_{xy}]$ flow extracted from the data as a function of the magnetic field at $T = 1.6$ K is also shown (solid black line).

be enhanced considerably over the band value $g^*\mu_B B$ through the *sp-d* exchange interaction between itinerant carriers and localized magnetic moments, as observed in various dilute magnetic semiconductors, primarily doped with Mn but also with Fe^{3+} ions [59]. By applying *g*-factor engineering, the TPT might be shifted to much weaker magnetic fields and higher temperatures. The renormalization group flow for the QAH type (3) in paramagnetic $(Bi,Sb)_2Se_3$ film [Figs. 1(c) and 1(f)] can be understood in terms of universal QAH phenomena as previously discussed in type (1) in ferromagnetic $(Bi,Sb)_2Te_3$ films [8,25,56].

IV. CONCLUSION

We have performed a comprehensive study of topological phase transitions based on Fe-doped $(Bi,Sb)_2Se_3$ thin films, which are driven by structural modification, doping, and external magnetic and electric fields. We found that topological phase transition occurs from a 3D TI to a 2D insulator by Fe doping owing to localization by magnetic disorder. The 2D insulator is changed to the QAH state by an external magnetic field owing to a large Zeeman splitting and suppression of the magnetic disorder. Demonstration of the magnetic-field-induced TPT toward the QAH state in a Bi_2Se_3-based 3D TI sheds light on perspectives of the QAH physics and expands it to a broader class of paramagnetic TI materials with properties that can be controlled by *g*-factor engineering.

ACKNOWLEDGMENTS

This work was partly supported by CREST (Grants No. JPMJCR18T1 and No. JPMJCR18T2), the Japan Science and Technology Agency, a Grant-in-Aid for Scientific Research on Innovative Areas (Grant No. JP15H05853), and a Grant-in-Aid for Young Scientists (A) (Grant No. 16H05981). Y.S. was supported by the Kato Foundation for Promotion of Science (Grant No. KS-2914). The work in Poland was funded by the Foundation for Polish Science through the IRA Programme financed by the EU within SG OP Programme. We thank NEOARK Corporation for the use of photolithography equipment for device fabrication.

[1] M. Z. Hasan and C. L. Kane, Colloquium: Topological insulators, Rev. Mod. Phys. **82**, 3045 (2010).

[2] X. L. Qi and S. C. Zhang, Topological insulators and superconductors, Rev. Mod. Phys. **83**, 1057 (2011).

[3] Y. Ando, Topological insulator materials, J. Phys. Soc. Jpn. **82**, 102001 (2013).

[4] Y. Zhang, K. He, C. Z. Chang, C. L. Song, L. L. Wang, X. Chen, J. F. Jia, Z. Fang, X. Dai, W. Y. Shan *et al.*, Crossover of the three-dimensional topological insulator Bi_2Se_3 to the two-dimensional limit, Nat. Phys. **6**, 584 (2010).

[5] T. Sato, K. Segawa, K. Kosaka, S. Souma, K. Nakayama, K. Eto, T. Minami, and Y. Ando, Unexpected mass acquisition of Dirac fermions at the quantum phase transition of a topological insulator, Nat. Phys. **7**, 840 (2011).

[6] M. Brahlek, N. Bansal, N. Koirala, S. Y. Xu, M. Neupane, C. Liu, M. Z. Hasan, and S. Oh, Topological-Metal to Band-Insulator Transition in $(Bi_{1-x}In_x)_2Se_3$ Thin Films, Phys. Rev. Lett. **109**, 186403 (2012).

[7] J. Zhang, C. Z. Chang, P. Tang, Z. Zhang, X. Feng, K. Li, L. Wang, X. Chen, C. Liu, W. Duan *et al.*, Topology-driven magnetic quantum phase transition in topological insulators, Science **339**, 1582 (2013).

[8] X. Kou, L. Pan, J. Wang, Y. Fan, E. S. Choi, W. L. Lee, T. Nie, K. Murata, Q. Shao, S. C. Zhang, and K. L. Wang, Metal-to-insulator switching in quantum anomalous Hall states, Nat. Commun. **6**, 8474 (2015).

[9] Y. Feng, X. Feng, Y. Ou, J. Wang, C. Liu, L. Zhang, D. Zhao, G. Jiang, S. C. Zhang, K. He *et al.*, Observation of the Zero Hall Plateau in a Quantum Anomalous Hall Insulator, Phys. Rev. Lett. **115**, 126801 (2015).

[10] C. Z. Chang, W. Zhao, J. Li, J. K. Jain, C. Liu, J. S. Moodera, and M. H. W. Chan, Observation of the Quantum Anomalous Hall Insulator to Anderson Insulator Quantum Phase Transition and Its Scaling Behavior, Phys. Rev. Lett. **117**, 126802 (2016).

[11] M. Mogi, M. Kawamura, R. Yoshimi, A. Tsukazaki, Y. Kozuka, N. Shirakawa, K. S. Takahashi, M. Kawasaki, and Y. Tokura, A magnetic heterostructure of topological insulators as a candidate for an axion insulator, Nat. Mater. **16**, 516 (2017).

[12] M. Kawamura, M. Mogi, R. Yoshimi, A. Tsukazaki, Y. Kozuka, K. S. Takahashi, M. Kawasaki, and Y. Tokura, Topological quantum phase transition in magnetic topological insulator upon magnetization rotation, Phys. Rev. B **98**, 140404(R) (2018).

[13] D. Xiao, J. Jiang, J. H. Shin, W. Wang, F. Wang, Y. F. Zhao, C. Liu, W. Wu, M. H. W. Chan, N. Samarth, and C. Z. Chang, Realization of the Axion Insulator State in Quantum Anomalous Hall Sandwich Heterostructures, Phys. Rev. Lett. **120**, 056801 (2018).

[14] S. Oh, The complete quantum Hall trio, Science **340**, 153 (2013).

[15] Y. Tokura, K. Yasuda, and A. Tsukazaki, Magnetic topological insulators, Nat. Rev. Phys. **1**, 126 (2019).

[16] C. Z. Chang and M. Li, Quantum anomalous Hall effect in time-reversal-symmetry breaking topological insulators, J. Phys.: Condens. Matter **28**, 123002 (2016).

[17] R. Yu, W. Zhang, H. J. Zhang, S. C. Zhang, X. Dai, and Z. Fang, Quantized anomalous Hall effect in magnetic topological insulators, Science **329**, 61 (2010).

[18] Y. Deng, Y. Yu, M. Z. Shi, Z. Guo, Z. Xu, J. Wang, X. H. Chen, and Y. Zhang, Quantum anomalous Hall effect in intrinsic magnetic topological insulator $MnBi_2Te_4$, Science **367**, 895 (2020).

[19] C. Liu, Y. Wang, H. Li, Y. Wu, Y. Li, J. Li, K. He, Y. Xu, J. Zhang, and Y. Wang, Robust axion insulator and Chern insulator phases in a two-dimensional antiferromagnetic topological insulator, Nat. Mater. (2020), doi: 10.1038/s41563-019-0573-3.

[20] W. Luo and X. L. Qi, Massive Dirac surface states in topological insulator/magnetic insulator heterostructures, Phys. Rev. B **87**, 085431 (2013).

[21] S. V. Eremeev, V. N. Men'shov, V. V. Tugushev, P. M. Echenique, and E. V. Chulkov, Magnetic proximity effect at

the three-dimensional topological insulator/magnetic insulator interface, Phys. Rev. B **88**, 144430 (2013).

[22] V. N. Men'shov, I. A. Shvets, and E. V. Chulkov, Interface effects on the magnetic-proximity-induced quantized Hall response in heterostructures based on three-dimensional topological insulators, Phys. Rev. B **99**, 115301 (2019).

[23] C. X. Liu, X. L. Qi, X. Dai, Z. Fang, and S. C. Zhang, Quantum Anomalous Hall Effect in $Hg_{1-y}Mn_yTe$ Quantum Wells, Phys. Rev. Lett. **101**, 146802 (2008).

[24] C. Z. Chang, J. Zhang, X. Feng, J. Shen, Z. Zhang, M. Guo, K. Li, Y. Ou, P. Wei, L. L. Wang *et al.*, Experimental observation of the quantum anomalous Hall effect in a magnetic topological insulator, Science **340**, 167 (2013).

[25] J. G. Checkelsky, R. Yoshimi, A. Tsukazaki, K. S. Takahashi, Y. Kozuka, J. Falson, M. Kawasaki, and Y. Tokura, Trajectory of the anomalous Hall effect towards the quantized state in a ferromagnetic topological insulator, Nat. Phys. **10**, 731 (2014).

[26] C. Z. Chang, W. Zhao, D. Y. Kim, H. Zhang, B. A. Assaf, D. Heiman, S. C. Zhang, C. Liu, M. H. W. Chan, and J. S. Moodera, High-precision realization of robust quantum anomalous Hall state in a hard ferromagnetic topological insulator, Nat. Mater. **14**, 473 (2015).

[27] S. Grauer, S. Schreyeck, M. Winnerlein, K. Brunner, C. Gould, and L. W. Molenkamp, Coincidence of superparamagnetism and perfect quantization in the quantum anomalous Hall state, Phys. Rev. B **92**, 201304(R) (2015).

[28] A. J. Bestwick, E. J. Fox, X. Kou, L. Pan, K. L. Wang, and D. Goldhaber-Gordon, Precise Quantization of the Anomalous Hall Effect Near Zero Magnetic Field, Phys. Rev. Lett. **114**, 187201 (2015).

[29] R. Watanabe, R. Yoshimi, M. Kawamura, M. Mogi, A. Tsukazaki, X. Z. Yu, K. Nakajima, K. S. Takahashi, M. Kawasaki, and Y. Tokura, Quantum anomalous Hall effect driven by magnetic proximity coupling in all-telluride based heterostructure, Appl. Phys. Lett. **115**, 102403 (2019).

[30] X. Feng, Y. Feng, J. Wang, Y. Ou, Z. Hao, C. Liu, Z. Zhang, L. Zhang, C. Lin, J. Liao *et al.*, Thickness dependence of the quantum anomalous Hall effect in magnetic topological insulator films, Adv. Mater. **28**, 6386 (2016).

[31] M. Salehi, H. Shapourian, I. T. Rosen, M. G. Han, J. Moon, P. Shibayev, D. Jain, D. Goldhaber-Gordon, and S. Oh, Quantum-Hall to insulator transition in ultra-low-carrier-density topological insulator films and a hidden phase of the zeroth Landau level, Adv. Mater. **31**, 1901091 (2019).

[32] Y. S. Kim, M. Brahlek, N. Bansal, E. Edrey, G. A. Kapilevich, K. Iida, M. Tanimura, Y. Horibe, S. W. Cheong, and S. Oh, Thickness-dependent bulk properties and weak antilocalization effect in topological insulator Bi_2Se_3, Phys. Rev. B **84**, 073109 (2011).

[33] A. A. Taskin, S. Sasaki, K. Segawa, and Y. Ando, Manifestation of Topological Protection in Transport Properties of Epitaxial Bi_2Se_3 Thin Films, Phys. Rev. Lett. **109**, 066803 (2012).

[34] G. Landolt, S. Schreyeck, S. V. Eremeev, B. Slomski, S. Muff, J. Osterwalder, E. V. Chulkov, C. Gould, G. Karczewski, K. Brunner *et al.*, Spin Texture of Bi_2Se_3 Thin Films in the Quantum Tunneling Limit, Phys. Rev. Lett. **112**, 057601 (2014).

[35] H. Zhang, C. X. Liu, X. L. Qi, X. Dai, Z. Fang, and S. C. Zhang, Topological insulators in Bi_2Se_3, Bi_2Te_3 and Sb_2Te_3 with a single Dirac cone on the surface, Nat. Phys. **5**, 438 (2009).

[36] Y. L. Chen, J. H. Chu, J. G. Analytis, Z. K. Liu, K. Igarashi, H. H. Kuo, X. L. Qi, S. K. Mo, R. G. Moore, D. H. Lu *et al.*, Massive Dirac fermion on the surface of a magnetically doped topological insulator, Science **329**, 659 (2010).

[37] L. A. Wray, S. Y. Xu, Y. Xia, D. Hsieh, A. V. Fedorov *et al.*, A topological insulator surface under strong Coulomb, magnetic and disorder perturbations, Nat. Phys. **7**, 32 (2011).

[38] M. R. Scholz, J. Sánchez-Barriga, D. Marchenko, A. Varykhalov, A. Volykhov, L. V. Yashina, and O. Rader, Tolerance of Topological Surface States towards Magnetic Moments: Fe on Bi_2Se_3, Phys. Rev. Lett. **108**, 256810 (2012).

[39] J. Honolka, A. A. Khajetoorians, V. Sessi, T. O. Wehling, S. Stepanow *et al.*, In-Plane Magnetic Anisotropy of Fe Atoms on Bi_2Se_3(111), Phys. Rev. Lett. **108**, 256811 (2012).

[40] X. F. Kou, W. J. Jiang, M. R. Lang, F. X. Xiu, L. He, Y. Wang, Y. Wang, X. X. Yu, A. V. Fedorov, P. Zhang, and K. L. Wang, Magnetically doped semiconducting topological insulators, J. Appl. Phys. **112**, 063912 (2012).

[41] M. Brahlek, N. Koirala, M. Salehi, N. Bansal, and S. Oh, Emergence of Decoupled Surface Transport Channels in Bulk Insulating Bi_2Se_3 Thin Films, Phys. Rev. Lett. **113**, 026801 (2014).

[42] Y. Y. Li, G. Wang, X. G. Zhu, M. H. Liu, C. Ye, X. Chen, Y. Y. Wang, K. He, L. L. Wang, X. C. Ma *et al.*, Intrinsic topological insulator Bi_2Te_3 thin films on Si and their thickness limit, Adv. Mater. **22**, 4002 (2010).

[43] See Supplemental Material at http://link.aps.org/supplemental/10.1103/PhysRevMaterials.4.044202 for additional information on experimental methods, characterization of electronic band structure by ARPES, detailed data of electric transport measurements, and structural characterization [60–74].

[44] Y. Satake, J. Shiogai, D. Takane, K. Yamada, K. Fujiwara, S. Souma, T. Sato, T. Takahashi, and A. Tsukazaki, Fermi-level tuning of the Dirac surface state in $(Bi_{1-x}Sb_x)_2Se_3$ thin films, J. Phys.: Condens. Matter **30**, 085501 (2018).

[45] Y. Satake, J. Shiogai, K. Fujiwara, and A. Tsukazaki, Effect of the depletion region in topological insulator heterostructures for ambipolar field-effect transistors, Phys. Rev. B **98**, 125415 (2018).

[46] J. M. Zhang, W. Zhu, Y. Zhang, D. Xiao, and Y. Yao. Tailoring Magnetic Doping in the Topological Insulator Bi_2Se_3, Phys. Rev. Lett. **109**, 266405 (2012).

[47] M. G. Vergniory, M. M. Otrokov, D. Thonig, M. Hoffmann, I. V. Maznichenko, M. Geilhufe, X. Zubizarreta, S. Ostanin, A. Marmodoro, J. Henk, W. Hergert, I. Mertig, E. V. Chulkov, and A. Ernst, Exchange interaction and its tuning in magnetic binary chalcogenides, Phys. Rev. B **89**, 165202 (2014).

[48] P. A. Lee and T. V. Ramakrishnan, Disordered electronic systems, Rev. Mod. Phys. **57**, 287 (1985).

[49] E. Abrahams, S. V. Kravchenko, and M. P. Sarachik, Metallic behavior and related phenomena in two dimensions, Rev. Mod. Phys. **73**, 251 (2001).

[50] J. Liao, Y. Ou, X. Feng, S. Yang, C. Lin, W. Yang, K. Wu, K. He, X. Ma, Q. K. Xue, and Y. Li, Observation of Anderson Localization in Ultrathin Films of Three-Dimensional Topological Insulators, Phys. Rev. Lett. **114**, 216601 (2015).

[51] C. X. Liu, H. J. Zhang, B. Yan, X. L. Qi, T. Frauenheim, X. Dai, Z. Fang, and S. C. Zhang, Oscillatory crossover from two-dimensional to three-dimensional topological insulators, Phys. Rev. B **81**, 041307(R) (2010).

[52] K. Kobayashi, Y. Yoshimura, K. I. Imura, and T. Ohtsuki, Dimensional crossover of transport characteristics in topological insulator nanofilms, Phys. Rev. B **92**, 235407 (2015).

[53] M. Liu, J. Zhang, C. Z. Chang, Z. Zhang, and X. Feng, K. Li, K. He, L.-l. Wang, X. Chen, X. Dai, Z. Fang, Q.-K. Xue, X. Ma, and Y. Wang, Crossover between Weak Antilocalization and Weak Localization in a Magnetically Doped Topological Insulator, Phys. Rev. Lett. **108**, 036805 (2012).

[54] K. Nomura and N. Nagaosa, Surface-Quantized Anomalous Hall Current and the Magnetoelectric Effect in Magnetically Disordered Topological Insulators, Phys. Rev. Lett. **106**, 166802 (2011).

[55] M. Mogi, R. Yoshimi, A. Tsukazaki, K. Yasuda, Y. Kozuka, K. S. Takahashi, M. Kawasaki, and Y. Tokura, Magnetic modulation doping in topological insulators toward higher-temperature quantum anomalous Hall effect, Appl. Phys. Lett. **107**, 182401 (2015).

[56] S. Grauer, K. M. Fijalkowski, S. Schreyeck, M. Winnerlein, K. Brunner, R. Thomale, C. Gould, and L. W. Molenkamp, Scaling of the Quantum Anomalous Hall Effect as an Indicator of Axion Electrodynamics, Phys. Rev. Lett. **118**, 246801 (2017).

[57] J. G. Analytis, R. D. McDonald, S. C. Riggs, J. H. Chu, G. S. Boebinger, and I. R. Fisher, Two-dimensional surface state in the quantum limit of a topological insulator, Nat. Phys. **6**, 960 (2010).

[58] Y. S. Fu, T. Hanaguri, K. Igarashi, M. Kawamura, M. S. Bahramy, and T. Sasagawa, Observation of Zeeman effect in topological surface state with distinct material dependence, Nat. Commun. **7**, 10829 (2016).

[59] J. G. Rousset, J. Papierska, W. Pacuski, A. Golnik, M. Nawrocki, W. Stefanowicz, S. Stefanowicz, M. Sawicki, R. Jakieła, T. Dietl *et al.*, Relation between exciton splittings, magnetic circular dichroism, and magnetization in wurtzite $Ga_{1-x}Fe_xN$, Phys. Rev. B **88**, 115208 (2013).

[60] C. L. Song, Y. P. Jiang, Y. L. Wang, Z. Li, L. Wang, K. He, X. Chen, X. C. Ma, and Q. K. Xue, Gating the charge state of single Fe dopants in the topological insulator Bi_2Se_3 with a scanning tunneling microscope, Phys. Rev. B **86**, 045441 (2012).

[61] M. M. Yee, Z. H. Zhu, A. Soumyanarayanan, Y. He, C. L. Song, E. Pomjakushina, Z. Salman, A. Kanigel, K. Segawa, Y. Ando, and J. E. Hoffman, Spin-polarized quantum well states on $Bi_{2-x}Fe_xSe_3$, Phys. Rev. B **91**, 161306(R) (2015).

[62] S. Awaji, K. Watanabe, H. Oguro, H. Miyazaki, S. Hanai, T. Tosaka, and S. Ioka, First performance test of a 25 T cryogen-free superconducting magnet, Supercond. Sci. Technol. **30**, 065001 (2017).

[63] Y. Jiang, Y. Wang, M. Chen, Z. Li, C. Song, K. He, L. Wang, X. Chen, X. Ma, and Q. K. Xue, Landau Quantization and the Thickness Limit of Topological Insulator Thin Films of Sb_2Te_3, Phys. Rev. Lett. **108**, 016401 (2012).

[64] J. Zhang, C. Z. Chang, Z. Zhang, J. Wen, X. Feng, K. Li, M. Liu, K. He, L. Wang, X. Chen *et al.*, Band structure engineering in $(Bi_{1-x}Sb_x)_2Te_3$ ternary topological insulators, Nat. Commun. **2**, 574 (2011).

[65] J. Linder, T. Yokoyama, and A. Sudbø, Anomalous finite size effects on surface states in the topological insulator Bi_2Se_3, Phys. Rev. B **80**, 205401 (2009).

[66] H. Jin, J. Im, and A. J. Freeman, Topological and magnetic phase transitions in Bi_2Se_3 thin films with magnetic impurities, Phys. Rev. B **84**, 134408 (2011).

[67] P. Kacman, Spin interactions in diluted magnetic semiconductors and magnetic semiconductor structures, Semicond. Sci. Technol. **16**, R25 (2001).

[68] T. Dietl, (Diluted) Magnetic Semiconductor, in *Handbook on Semiconductors*, edited by M. Balkanski (Elsevier, Amsterdam, 1994), Vol. 3b, p. 1251.

[69] J. K. Furdyna, Diluted magnetic semiconductors, J. Appl. Phys. **64**, R29 (1988).

[70] A. Twardowski, K. Pakula, I. Perez, P. Wise, and J. E. Crow, Magnetoreflectance and magnetization of the semimagnetic semiconductor $Cd_{1-x}Fe_xSe$, Phys. Rev. B **42**, 7567 (1990).

[71] D. Kim, S. Cho, N. P. Butch, P. Syers, K. Kirshenbaum, S. Adam, J. Paglione, and M. S. Fuhrer, Surface conduction of topological Dirac electrons in bulk insulating Bi_2Se_3, Nat. Phys. **8**, 459 (2012).

[72] I. Lee, C. K. Kim, J. Lee, S. J. L. Billinge, R. Zhong, J. A. Schneeloch, T. Liu, T. Valla, J. M. Tranquada, G. Gu, and J. C. Séamus Davis, Imaging Dirac-mass disorder from magnetic dopant atoms in the ferromagnetic topological insulator $Cr_x(Bi_{0.1}Sb_{0.9})_{2-x}Te_3$, Proc. Natl. Acad. Sci. USA **112**, 1316 (2015).

[73] R. Akiyama, K. Sumida, S. Ichinokura, R. Nakanishi, A. Kimura, K. A. Kokh, O. E. Tereshchenko, and S. Hasegawa, Shubnikov-de Haas oscillations in p and n-type topological insulator $(Bi_xSb_{1-x})_2Te_3$, J. Phys.: Condens. Matter **30**, 265001 (2018).

[74] H. M. N. Vasconcelos, M. Eddrief, Y. Zheng, D. Demaille, S. Hidki, E. Fonda, A. Novikova, J. Fujii, P. Torelli, B. R. Salles *et al.*, Magnetically hard Fe_3Se_4 embedded in Bi_2Se_3 topological insulator thin films grown by molecular beam epitaxy, ACS Nano **10**, 1132 (2016).